Journal of Physics: Condensed Matter

PAPER

# Crystal structures and phase relationships in magnetostrictive $Tb_{1-x}Dy_xCo_2$ system

To cite this article: Tieyan Chang *et al* 2020 *J. Phys.: Condens. Matter* **32** 135802



IOP Publishing Journal of Physics: Condensed Matter
J. Phys.: Condens. Matter **32** (2020) 135802 (8pp) https://doi.org/10.1088/1361-648X/ab5cc9

# Crystal structures and phase relationships in magnetostrictive $Tb_{1-x}Dy_xCo_2$ system

**Tieyan Chang[1,2,5], Chao Zhou[1,5], Jingwen Mi[1], Kaiyun Chen[1], Fanghua Tian[1], Yu-Sheng Chen[2], SuYin Grass Wang[2], Yang Ren[3], Dennis E Brown[4], Xiaoping Song[1] and Sen Yang[1]**

[1] School of Science, MOE Key Laboratory for Nonequilibrium Synthesis and Modulation of Condensed Matter, Xi'an Jiaotong University, Xi'an 710049, People's Republic of China
[2] NSF's ChemMatCARS, The University of Chicago, Lemont, IL 60439, United States of America
[3] X-ray Science Division, Advanced Photon Source, Argonne National Laboratory, Lemont, IL 60439, United States of America
[4] Department of Physics, Northern Illinois University, DeKalb, IL 60115, United States of America

E-mail: yang.sen@xjtu.edu.cn

Received 2 October 2019, revised 19 November 2019
Accepted for publication 28 November 2019
Published 30 December 2019

**Abstract**

The crystal structures and phase relationships of $Tb_{1-x}Dy_xCo_2$ alloys with $0 \leqslant x \leqslant 1$ were investigated by synchrotron-based high-resolution x-ray powder diffraction. Three different crystal structures are observed in the system: all the compositions show cubic structure with space group $Fd\bar{3}m$ at temperatures above the Curie temperature $T_C$; the Tb-rich side sample shows a rhombohedral structure with space group $R\bar{3}m$ and the Dy-rich side sample has a tetragonal $I4_1/amd$ space group. *In situ* measurements on the intermediate compound $Tb_{0.3}Dy_{0.7}Co_2$ show a rhombohedral to tetragonal structural transition, and the two phases coexist from 99 K to 111 K, where the so-called magnetic morphotropic phase boundary (MPB) is found. The coexisting phases are believed to induce the anomalous magnetostrictive effect in the MPB regime.

Keywords: crystal structure, laves phase, MPB, rietveld, synchrotron

Supplementary material for this article is available online

(Some figures may appear in colour only in the online journal)

## 1. Introduction

The Laves phases $RT_2$ (R = Rare-earth and T = Co, Fe) have drawn lots of interests for decades due to their outstanding magnetic properties [1–4]. This alloy family was believed to crystallize in a $MgCu_2$-type cubic phase, but now it is known that the magnetic phase transitions in the systems are accompanied by structural changes, and non-cubic phases are achieved at temperatures below their Curie temperature ($T_C$) [5–8]. In $Tb_{1-x}Dy_xCo_2$ [9], the high-temperature cubic phase transforms to rhombohedral (Tb-rich) symmetry and to tetragonal (Dy-rich) symmetry at low temperature, forming a phase boundary between the two non-cubic phases with a triple point. The magnetostrictive property is enhanced at this boundary, which is called the magnetic morphotropic phase boundary (MPB) [9]. Similar enhanced magnetostrictive response is observed and reported in other $RT_2$ systems [10–14]. The most common phases that a magnetic MPB separates are the rhombohedral phase ($\boldsymbol{M_S} \parallel [1\,1\,1]$ below $T_C$) and tetragonal phase ($\boldsymbol{M_S} \parallel [0\,0\,1]$ below $T_C$) [9–15]. The rhombohedral phase is easier to be distinguished from the high-temperature cubic phase than the tetragonal phase because the distortion along [1 1 1] direction is relatively stronger [16, 17]. However, the tetragonal phase is difficult to detect due to the small distortion along [0 0 1] ($\varepsilon < 10^{-3}$) and the limited resolution of instruments e.g. the in-house x-ray diffraction [7, 8]. The tetragonal distortion was detected and reported in $NdCo_2$ by neutron powder diffraction [5, 6] much later than

[5] TC and CZ contribute equally to this work.

 

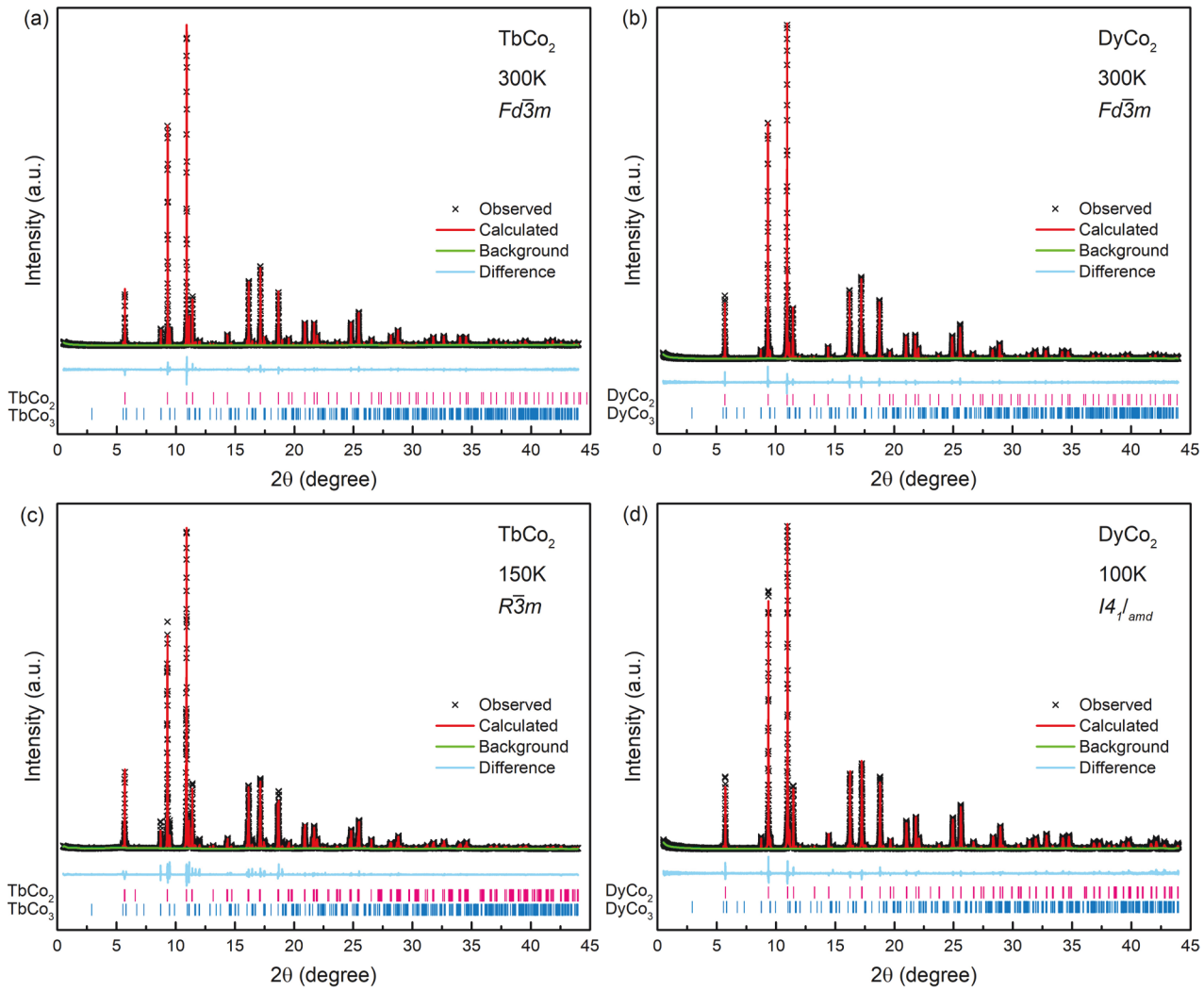


**Figure 1.** The refined XRD patterns for the samples: (a) $TbCo_2$ and (b) $DyCo_2$ show a cubic structure with space group $Fd\bar{3}m$ at 300 K. (c) $TbCo_2$ shows a $R\bar{3}m$ rhombohedral structure at 150 K and (d) $DyCo_2$ has a tetragonal structure with $I4_1/amd$ at 100 K. The background and difference are shown below the observed (cross) and calculated (red line) intensities, and the calculated Bragg peaks positions are shown by short bars at the bottom.

the rhombohedral phase. The magnetic field-induced and pressure-induced tetragonal distortions are reported [18–20] by using high-energy synchrotron x-ray.

Based on the prior researches [9, 10], the crystallography of the $RT_2$ system influences the physical properties of the alloys, especially their magnetostrictive property. Therefore, it is important to understand the crystal structures while studying the basic magnetism and magnetostrictive effect of the $RT_2$ alloys. However, many of recent works focus on the terminal binary compounds of $RT_2$ systems, but detailed studies on the structures of the ternary compounds by doping different rare-earth elements, especially the compounds near the magnetic MPB regime, are still rare.

In this work, we report the study on the crystal structures of the magnetic MPB carrier $Tb_{1-x}Dy_xCo_2$ system using the synchrotron-based high-resolution x-ray powder diffraction (HR-XRD) with Rietveld refinements. *In situ* measurements were performed on $Tb_{0.3}Dy_{0.7}Co_2$ from 260 K to 90 K to study the phase evolution. The first-order magnetoelastic phase transitions from cubic to rhombohedral to tetragonal structure is presented and detailed information of crystal structures are presented, which provide the basic data for understanding the physics of the $RT_2$ compounds and for further developing high-performance magnetostrictive materials.

## 2. Experiments

$Tb_{1-x}Dy_xCo_2$ ($0 \leqslant x \leqslant 1$) polycrystalline samples were synthesized by arc-melting in argon environment with 99.9 wt.% pure Tb, Dy, and Co. The ingots were melted six times to ensure the homogeneity. The ingots were sealed in evacuated quartz tube and annealed at 1000 °C for 48 h. Magnetic measurements were performed by a superconducting quantum interference device magnetometer (SQUID, Quantum Design). Well-ground powder samples were sealed in Kapton capillaries for *in situ* HR-XRD measurements with $\lambda = 0.4142$ Å at beamline 11-BM-B at the Advanced Photon Source, Argonne National Laboratory. The crystal structures were refined by

**Table 1.** Structures and refined parameters for $TbCo_2$ and $DyCo_2$ at room temperature and low temperatures.

| Sample | $TbCo_2$ | $DyCo_2$ |
|---|---|---|
| Temperature (K) | 300 ($T > T_C$) | 300 ($T > T_C$) |
| Structure type | $MgCu_2$ | $MgCu_2$ |
| Space group | $Fd\bar{3}m$ | $Fd\bar{3}m$ |
| Lattice parameter (Å) | $a = 7.22403$ (1) | $a = 7.18569$ (1) |
| Volume of cell (Å$^3$) | $V = 376.998$ (1) | $V = 371.028$ (1) |
| Calculated density (g cm$^{-3}$) | 9.753 | 10.039 |
| Reliability factors | $R_p = 9.59\%$ | $R_p = 10.85\%$ |
| | $R_{wp} = 11.82\%$ | $R_{wp} = 13.89\%$ |
| | $\chi^2 = 0.895$ | $\chi^2 = 0.906$ |

Atomic parameters

| $TbCo_2$ ($Fd\bar{3}m$) | | | | $DyCo_2$ ($Fd\bar{3}m$) | | | |
|---|---|---|---|---|---|---|---|
| Atom | Wyckoff | Position | Occ. | Atom | Wyckoff | Position | Occ. |
| Tb | 8a | 1/8,1/8,1/8 | 1 | Dy | 8a | 1/8,1/8,1/8 | 1 |
| Co | 16d | 1/2,1/2,1/2 | 1 | Co | 16d | 1/2,1/2,1/2 | 1 |

| Sample | $TbCo_2$ | $DyCo_2$ |
|---|---|---|
| Temperature (K) | 150 ($T < T_C$) | 100 ($T < T_C$) |
| Structure type | $TbFe_2$ | $NdCo_2$ |
| Space group | $R\bar{3}m$ | $I4_1/amd$ |
| Lattice parameter (Å) | $a = 5.09673$ (2) | $a = 5.07838$ (1) |
| | $c = 12.55179$ (5) | $c = 7.16754$ (4) |
| | $\gamma = 120°$ | |
| Volume of cell (Å$^3$) | $V = 282.371$ (3) | $V = 184.846$ (2) |
| Calculated density (g cm$^{-3}$) | 9.766 | 10.075 |
| Reliability factors | $R_p = 8.34\%$ | $R_p = 10.34\%$ |
| | $R_{wp} = 12.42\%$ | $R_{wp} = 12.97\%$ |
| | $\chi^2 = 1.65$ | $\chi^2 = 0.825$ |

Atomic parameters

| $TbCo_2$ ($R\bar{3}m$) | | | | $DyCo_2$ ($I4_1/amd$) | | | |
|---|---|---|---|---|---|---|---|
| Atom | Wyckoff | Position | Occ. | Atom | Wyckoff | Position | Occ. |
| Tb | 6c | 0,0,0.1256 | 1 | Dy | 4b | 1/2,3/4,3/8 | 1 |
| Co1 | 3b | 0,0,1/2 | 1 | Co | 8c | 3/4,3/4,3/4 | 1 |
| Co2 | 9e | 1/2,0,0 | 1 | | | | |

using the Rietveld algorithm [21, 22] as implemented in the software packages GSAS and EXPGUI [23, 24].

## 3. Results and discussions

The observed and calculated XRD patterns of the terminal binary compounds $TbCo_2$ and $DyCo_2$ are shown in figures 1(a) and (b), respectively. The results indicate that the system has a $MgCu_2$-type cubic phase with space group $Fd\bar{3}m$ (no. 223) at room temperature. The size of the crystal lattice decreasing with increasing Dy's proportion. (The lattice constant as a function of Dy content at room temperature is shown in figure S1 (stacks.iop.org/JPhysCM/32/135802/mmedia).) The low-temperature XRD were performed on $TbCo_2$ at 150 K and $DyCo_2$ at 100 K, which are all below their respective $T_C$. The refined patterns are displayed in figures 1(c) and 1(d), and the crystallographic information for $TbCo_2$ and $DyCo_2$ compounds are listed in table 1. The refined XRD patterns clearly show that at temperatures below $T_C$, the $TbCo_2$ crystallizes in a rhombohedral structure with space group $R\bar{3}m$ (no. 166), while the $DyCo_2$ is in a tetragonal structure with space group $I4_1/amd$ (no. 141). The easy magnetization directions $\boldsymbol{M_S}$ of the two phases are along the [1 1 1] and [0 0 1] directions of the cubic cell, respectively [9]. The cubic peaks split into non-cubic peaks with very close $2\theta$ angles because the distortions are small and the non-cubic structures are very close to the cubic motherphase, which makes them look quite 'cubic', and it would be difficult to observe the differences without the help of techniques with high spatial resolution, such as neutron and synchrotron diffraction [7, 25].

It turns out that an impure phase of $RCo_3$ with space group $R3\,m$ exists in all samples at measured temperatures. This impurity is modelled and its proportion gained from the refinements is about ~8 wt.%, and it does not show obvious change at different temperatures. During the sample preparation, impurities like $RCo_3$ and $R_4Co_3$ *et al* could form and

**Table 2.** Bond lengths (Å) and bond angles (°) for $TbCo_2$ and $DyCo_2$ at room temperature and low temperature.

| | $TbCo_2$ (300 K) | | $DyCo_2$ (300 K) |
|---|---|---|---|
| Tb–Tb | 3.128 10(0) × 4 | Dy–Dy | 3.111 50(0) × 4 |
| Tb–Co | 2.994 93(0) × 12 | Dy–Co | 2.979 03(0) × 12 |
| Co–Co | 2.554 08(0) × 6 | Co–Co | 2.540 53(0) × 6 |
| Tb–Tb–Tb | 109.471(0) | Dy–Dy–Dy | 109.471(0) |
| Tb–Tb–Co | 150.504(0) | Dy–Dy–Co | 150.504(0) |
| | 100.025(0) | | 100.025(0) |
| | 58.518(0) | | 58.518(0) |
| Tb–Co–Tb | 117.036(0) | Dy–Co–Dy | 117.036(0) |
| | 62.964(0) | | 62.964(0) |
| Co–Tb–Co | 144.903(0) | Co–Dy–Co | 144.903(0) |
| | 117.036(0) | | 117.036(0) |
| | 95.216(0) | | 95.216(0) |
| | 50.479(0) | | 50.479(0) |
| | $TbCo_2$ (150 K) | | $DyCo_2$ (100 K) |
| Tb–Tb | 3.149 82(1) × 1 | Dy–Dy | 3.107 77(1) × 4 |
| | 3.119 02(1) × 3 | Dy–Co | 2.972 63(1) × 4 |
| Tb–Co1 | 2.987 68(1) × 3 | | 2.976 87(1) × 2 |
| Tb–Co2 | 2.995 75(1) × 6 | Co–Co | 2.536 65(1) × 4 |
| Co1–Co2 | 2.557 55(1) × 6 | | 2.539 13(1) × 2 |
| Co2–Co2 | 2.548 37(1) × 4 | Dy–Dy–Dy | 109.577(0) |
| | 2.995 28(1) × 3 | | 109.418(0) |
| Tb–Tb–Tb | 109.579(0) | Dy–Dy–Co | 150.509(0) |
| | 109.363(0) | | 150.494(0) |
| Tb–Tb–Co1 | 150.671(0) | | 100.073(0) |
| | 99.966(0) | | 99.929(0) |
| | 58.535(0) | | 58.576(0) |
| Tb–Tb–Co2 | 150.58(0) | | 58.534(0) |
| | 150.38(0) | | 58.443(0) |
| | 100.057(0) | Co–Dy–Co | 144.968(0) |
| | 100.038(0) | | 144.897(0) |
| | 58.634(0) | | 144.845(0) |
| | 58.619(0) | | 117.019(0) |
| | 58.284(0) | | 95.287(0) |
| Co1–Tb–Co1 | 117.070(0) | | 95.197(0) |
| Co1–Tb–Co2 | 144.742(0) | | 95.164(0) |
| | 95.230(0) | | 50.565(0) |
| | 95.220(0) | | 50.474(0) |
| | 50.614(0) | | 50.436(0) |
| | 50.610(0) | Dy–Co–Dy | 117.069(0) |
| Co2–Tb–Co2 | 145.064(0) | | 117.019(0) |
| | 117.253(0) | | 62.981(0) |
| | 116.567(0) | | 62.931(0) |
| | 95.512(0) | Tb–Co1–Tb | 62.93(0) |
| | 94.901(0) | Tb–Co2–Tb | 117.253(0) |
| | 50.352(0) | | 116.567(0) |
| | 50.343(0) | | 63.433(0) |
| Tb–Co1–Tb | 117.07(0) | | 62.747(0) |

exist in the sample which are reported in other Laves systems [6, 26]. Hence, in the following sections we will focus on the main phase $RCo_2$.

At room temperature, the rare-earth (R) atoms occupy the 8a positions and Co atoms occupy the 16d sites. When cooling the samples to temperatures below their $T_C$, the R atoms in rhombohedral phase occupy the 6c sites (with $z = 0.1256$ for $TbCo_2$ at 150 K), and Co atoms occupy two different sites 3b and 9e; in the tetragonal phase, the R atoms occupy the 4b sites, while the Co atoms are in the 8c sites. The bond lengths and bond angles for the two binary compounds at room temperature and low temperatures are listed in table 2.

The crystal structure for the cubic phase is shown in figure 2(a1). The distances between two nearest neighbor Co atoms are all equal and they form top-to-top tetrahedrons in the cell, which are colored in red in the figures. When cooling

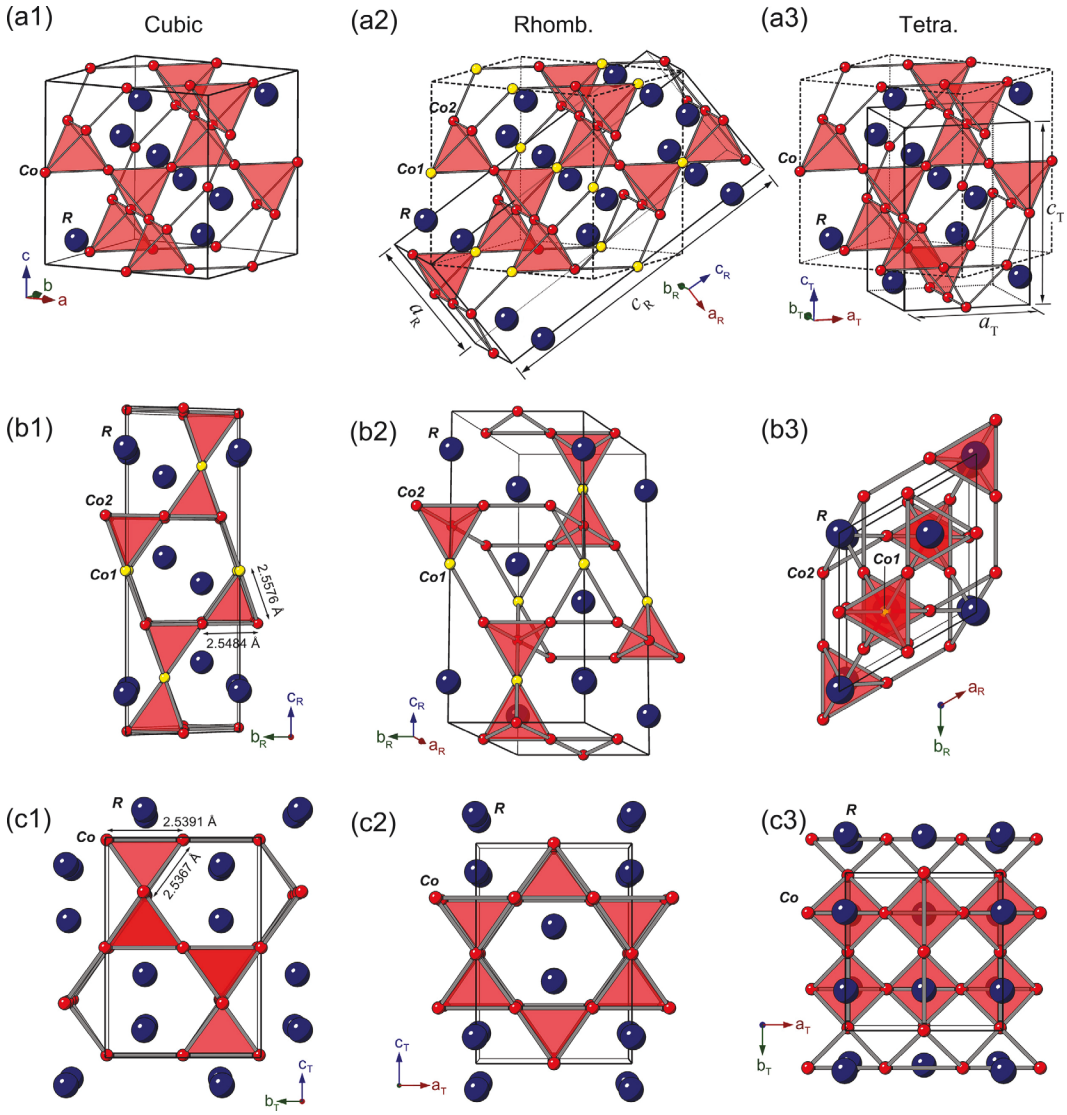


**Figure 2.** The crystal structures of the Laves phases $Tb_{1-x}Dy_xCo_2$: (a1) cubic ($Fd\bar{3}m$), (a2) rhombohedral ($R\bar{3}m$) in the hexagonal description, and (a3) tetragonal ($I4_1/amd$). The structure of rhombohedral cell is viewed along (b1) $\boldsymbol{a}_R$ axis, (b2) $\boldsymbol{b}_R^*$ axis and (b3) $\boldsymbol{c}_R$ axis. The structure of tetragonal cell is viewed along (c1) $\boldsymbol{a}_T$ axis, (c2) $\boldsymbol{b}_T$ axis and (c3) $\boldsymbol{c}_T$ axis. The 'rhomb.' and 'tetra.' in all the figures are short for 'rhombohedral' and 'tetragonal'.

the Tb-rich side samples to temperature $T < T_C$, the rhombohedral phase forms and the crystal structure of which is shown in figure 2(a2). The unit cell in the hexagonal description is drawn in black solid line and the original cubic cell is shown in black dotted line. In the rhombohedral lattice the Co atoms occupy two different sites: Co1 is the one at the top of tetrahedron along the $\boldsymbol{c}_R$ axis of the rhombohedral cell, and Co1 is colored in yellow in the figures; three Co2 are at the top of the tetrahedron bottom plane which is perpendicular to the $\boldsymbol{c}_R$ axis, and they are colored in red. The side views of the rhombohedral cell along its $\boldsymbol{a}_R$, $\boldsymbol{b}_R^*$ and $\boldsymbol{c}_R$ axes are shown in figures 2(b1)–(b3), respectively. From table 2 one can notice that the Co1–Co2 bond length in the cell is a little longer than that of Co2–Co2 bond, and this difference distorts the cell along the [1 1 1] direction of the cubic cell and results in the cubic to rhombohedral structural transition. For Dy-rich side compounds, the low-temperature phase crystallizes in the tetragonal structure and is shown in figure 2(a3). The side views of the tetragonal cell along the $\boldsymbol{a}_T$, $\boldsymbol{b}_T$ and $\boldsymbol{c}_T$ axes are shown in figures 2(c1)–(c3), respectively. In the tetragonal phase, it has two different bond lengths in the tetrahedrons: the two Co-Co bonds in the $\boldsymbol{a}_T\boldsymbol{b}_T$ plane show a longer bond length (~2.5391 Å for $DyCo_2$ at 100 K); the other two Co-Co bonds out-of-plane are shorter than the former bonds (~2.5367 Å for $DyCo_2$ at 100 K). The shorter bond lengths for the out-of-plane bonds make the cell compressed along the $\boldsymbol{c}_T$ axis and the pseudo-cubic lattice with $c/a < 1$ was detected [7, 18].

The crystal symmetry lowing occurs accompanying by the paramagnetic-ferrimagnetic phase transition at $T_C$. Because the system shows a tilted phase boundary between the rhombohedral and tetragonal phases, the enhanced magnetostrictive property could be achieved by either tuning composition or changing temperature. The composition $Tb_{0.3}Dy_{0.7}Co_2$ is selected for the following measurements, which shows enhanced field response near ~110 K [9]. The temperature-dependent ac magnetic susceptibility curve under H = 50 Oe

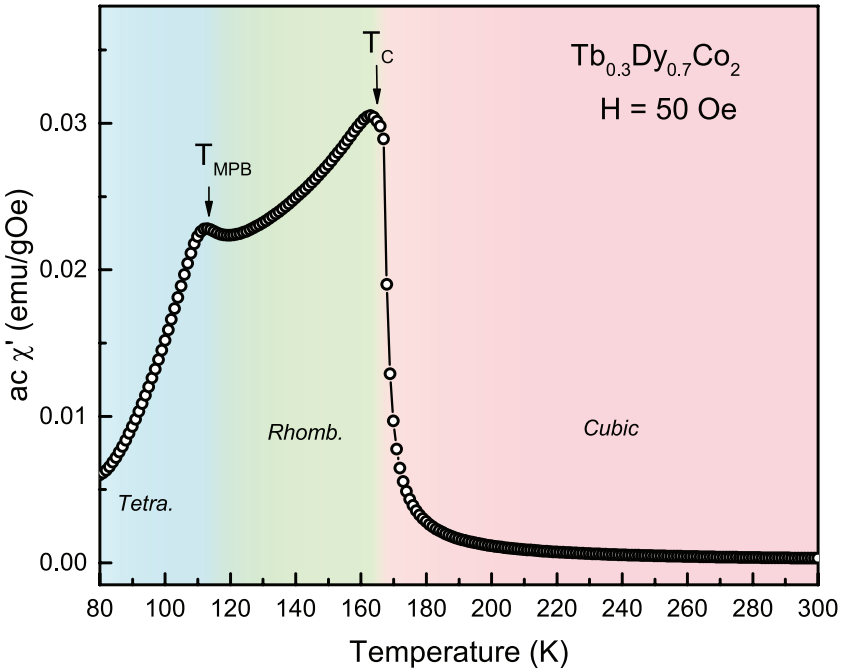


**Figure 3.** The temperature dependence of ac magnetic susceptibility for $Tb_{0.3}Dy_{0.7}Co_2$ under an applied mnetic field H = 50 Oe at 153 Hz.

at 153 Hz for $Tb_{0.3}Dy_{0.7}Co_2$ is shown in figure 3. The Curie temperature $T_C = 161$ K separates the disordered paramagnetic phase (at $T > T_C$) from the ordered ferrimagnetic phase (at $T < T_C$) where the increase in the magnetization observed upon cooling corresponds to the para-ferrimagnetic transition. The peak at 112 K is ascribed to the magnetoelastic rhombohedral to tetragonal transition where is defined as $T_{MPB}$ [9]. To further investigate the crystal structure evolution, *in situ* HR-XRD measurements were performed on $Tb_{0.3}Dy_{0.7}Co_2$ from 260 K down to 90 K in steps of $\Delta T = 3$ K.

In figure 4(a) we show the evolution of diffraction peaks at $2\theta = 10.96°$ for $Tb_{0.3}Dy_{0.7}Co_2$ sample on cooling. Because it is unreliable to distinguish elements with very close atomic numbers (e.g. Tb and Dy) using powder XRD, the site occupation factors (SOF) for the rare-earth atoms are not refined and fixed to their nominal ratios. Above the $T_C$ ~161 K, the diffraction peak is a single cubic peak which can be indexed as $(3\,1\,1)_C$ (here the footnote C stands for cubic and the same to the R for rhombohedral and T for tetragonal mentioned later). With the temperature going down, the peak shifts to higher angle because of the shrink of lattice on cooling. Then it splits into three peaks which can be indexed as rhombohedral $(1\,0\,-5)_R$, $(1\,1\,3)_R$ and $(2\,0\,1)_R$ below $T_C$, indicating a first-order magnetoelastic phase transition. And with the temperature continuingly going down, the three rhombohedral peaks change into different two peaks, which are indexed as tetragonal $(2\,1\,1)_T$ and $(1\,0\,3)_T$ peaks. The results demonstrate the structural phase transition in $Tb_{0.3}Dy_{0.7}Co_2$ sample during the cooling process, which is from cubic to rhombohedral then to tetragonal phase.

From the $(3\,1\,1)_C$ peak's evolution, it could be noticed that the transition from rhombohedral to tetragonal structure in the vicinity of $T_{MPB}$ ~ 112 K lasts for several kelvins. The transition here is slow and the system in this temperature regime is composed of coexisting rhombohedral and tetragonal phases. The enlarged patterns for the $(3\,1\,1)_C$ peak within the temperature range 93 K to 120 K is displayed in figure 4(b) and careful eye examination could notice that the diffraction spectra between 99 K and 111 K are not in pure rhombohedral or tetragonal phase, but show gently changes between the two phases. Adding the low-temperature tetragonal phase as a second phase to the rhombohedral phase could lead to an improvement in the refinement and a decrease of the R values. We show the result for the broad $(311)_C$ peaks at 105 K in figure 4(b), in which the peaks are fitted with rhombohedral $R3\,m$ space group accompanied by tetragonal $I4_1/amd$ space group. The refinement gives the fraction of 38.7 wt.% for the rhombohedral phase and 61.3 wt.% for the tetragonal phase. The amount of the two phases within this temperature range is shown in figure 4(d). The proportion of tetragonal phase increasing from ~10 wt.% at 111 K to more than 95 wt.% at 99 K, while the rhombohedral phase is correspondingly decreasing. Hence, the two phases coexisted within a rough temperature range 99 ~ 111 K, where defines the width of magnetic MPB range in $Tb_{0.3}Dy_{0.7}Co_2$.

Figures 5(a) and (b) show the temperature dependence of lattice parameters and cell volume, respectively. The lattice parameters of the rhombohedral and tetragonal structures are normalized to compare with high temperature cubic phase. The lattice parameters change obviously at $T_C$ and $T_{MPB}$, but the values of the changes are very small, which makes it undetectable using the in-house XRD. The cell volume displays large change at $T_C$ while it does not vary much at the rhombohedral to tetragonal transition near $T_{MPB}$, which

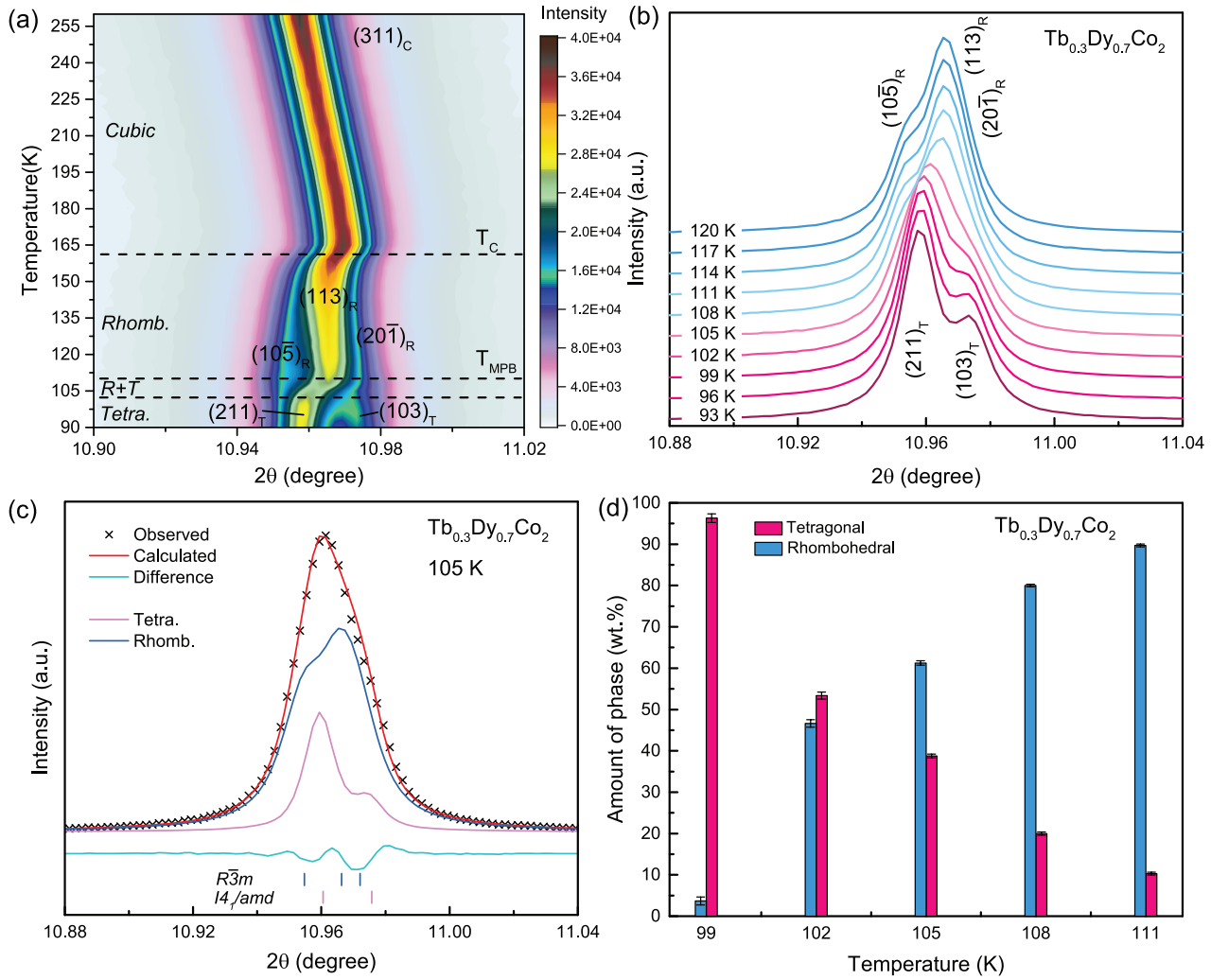


**Figure 4.** (a) The evaluation of $(3\,1\,1)_C$ peak of $Tb_{0.3}Dy_{0.7}Co_2$ on the cooling process. (b) The enlarged $(3\,1\,1)_C$ peak within temperature range 93 ~ 120 K. (c) The $(3\,1\,1)_C$ peak refined using coexisted rhombohedral and tetragonal phases. (d) The amount of the two phases within the temperature range.

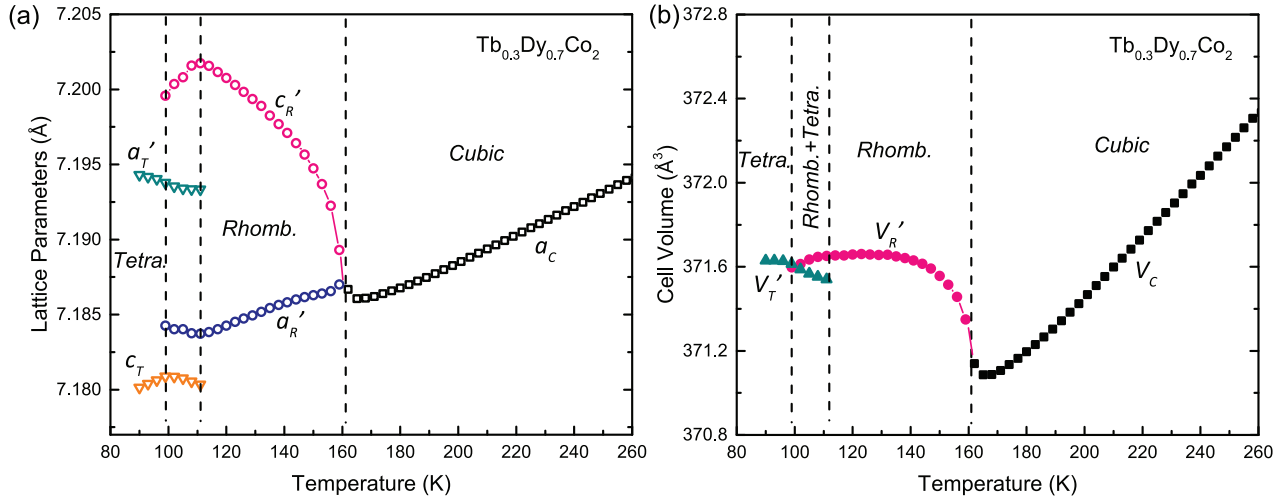


**Figure 5.** (a) The temperature dependence of lattice parameters for $Tb_{0.3}Dy_{0.7}Co_2$. (b) The temperature dependence of cell volume for $Tb_{0.3}Dy_{0.7}Co_2$. Here $a'_T = \sqrt{2}a_T$, $a'_R = \sqrt{2}a_R$, $c'_R = c_R/\sqrt{3}$, $V'_T = 2V_T$, and $V'_R = 2/\sqrt{3}V_R$.

is quite similar to the transition behaviors in $NdCo_2$ [6]. The results confirm the first-order magnetoelastic transitions with crystal symmetry changing at $T_C$ and $T_{MPB}$. In the MPB regime, the system is in bistable state with two crystal structures and two easy magnetization directions $\boldsymbol{M_S}$. The coexistence of the two states makes the crystal lattice unstable and easily to be driven by a small external magnetic field [9–11]. Hence, the coexisted rhombohedral and tetragonal phases induces the anomalous magnetostrictive effect near the MPB temperature.

## 4. Conclusion

In conclusion, the crystal structures and the first-order magnetoelastic phase transitions in the Laves compounds $Tb_{1-x}Dy_xCo_2$ ($0 \leqslant x \leqslant 1$) were investigated. The synchrotron-based HR-XRD results show that the system crystallizes in the cubic structure ($Fd\bar{3}m$) with $a = 7.224\,03(1) \sim 7.185\,69(1)$ Å at room temperature. When cooling the system below its $T_C$, a structural transition occurs accompanied by the para-ferrimagnetic phase transition, and the system changes from cubic to rhombohedral ($R\bar{3}m$) at Tb-rich side or tetragonal structure ($I4_1/amd$) at Dy-rich side. In the intermediate composition $Tb_{0.3}Dy_{0.7}Co_2$, it undergoes a rhombohedral to tetragonal phase transition below $T_C$ which is ascribed as the magnetic MPB. The *in situ* measurements reveal that the rhombohedral and tetragonal phases coexist within a rough temperature range from 99 to 111 K in $Tb_{0.3}Dy_{0.7}Co_2$, which is believed to induce the anomalous magnetostrictive effect at the MPB in $RT_2$ systems.

## Acknowledgments

This research was funded by the National Natural Science Foundation of China (Grants Nos. 51601140, 51701149), the Fundamental Research Funds for the Central Universities (China), the World-Class Universities (Disciplines), the National Science Basic Research Plan in the Shaanxi Province of China (2018JM5168), the Characteristic Development Guidance Funds for the Central Universities. Use of the Advanced Photon Source at Argonne National Laboratory was supported by the U. S. Department of Energy, Office of Science, Office of Basic Energy Sciences, under Contract No. DE-AC02-06CH11357. NSF's ChemMatCARS is supported by the National Science Foundation under Grant No. NSF/CHE-1834750.

## ORCID iDs

Tieyan Chang https://orcid.org/0000-0002-7434-3714
Chao Zhou https://orcid.org/0000-0001-7173-9636
Yu-Sheng Chen https://orcid.org/0000-0002-7646-7761
SuYin Grass Wang https://orcid.org/0000-0001-8474-9817
Sen Yang https://orcid.org/0000-0001-5784-2952

## References

[1] Chopra H and Wuttig M 2015 *Nature* **521** 340
[2] Adelsberg N, Weber Y, Yoffe A and Shilo D 2017 *Smart Mater. Struct.* **26** 065013
[3] Lv X, Or S, Liu W, Liu X and Zhang Z 2008 *J. Phys. D: Appl. Phys.* **42** 035002
[4] Guo Z, Zhang Z, Wang B, Zhao X, Geng D and Liu W 2001 *J. Phys. D: Appl. Phys.* **34** 884
[5] Ouyang Z, Wang F, Huang Q, Liu W, Xiao Y, Lynn J, Liang J and Rao G 2005 *Phys. Rev.* B **71** 064405
[6] Xiao Y, Huang Q, Ouyang Z, Lynn J, Liang J and Rao G 2006 *J. Alloys Compd.* **420** 29
[7] Yang S and Ren X 2008 *Phys. Rev.* B **77** 014407
[8] Barbara B, Giraud J P, Laforest J, Lemaire R, Siaud E and Schweizer J 1977 *Physica B+C* **86–8** 155
[9] Yang S *et al* 2010 *Phys. Rev. Lett.* **104** 197201
[10] Bergstrom R, Wuttig M Jr, Cullen J, Zavalij P, Briber R, Dennis C, Garlea V and Laver M 2013 *Phys. Rev. Lett.* **111** 017203
[11] Hu C, Yang T, Huang H, Hu J, Wang J, Shi Y, Shi D and Chen L 2016 *Appl. Phys. Lett.* **108** 141908
[12] Zhou C *et al* 2014 *Phys. Rev.* B **89** 100101
[13] Murtaza A, Yang S, Zhou C, Chang T, Chen K, Tian F, Song X, Suchomel M and Ren Y 2016 *Appl. Phys. Lett.* **109** 052904
[14] Ma T, Liu X, Gou J, Wang Y, Wu C, Zhou C, Wang Y, Yang S and Ren X 2019 *Phys. Rev. Mater.* **3** 034411
[15] Atzmony U and Dariel M 1976 *Phys. Rev.* B **13** 4006
[16] Dwight A and Kimbal C 1974 *Acta Cryst.* B **30** 2791
[17] Goldberg-Murmis V, Atzmony U and Dariel M 1980 *J. Mater. Sci.* **15** 127
[18] Nie Z, Yang S, Wang Y, Wang Z, Liu D and Ren Y 2013 *Appl. Phys. Lett.* **103** 111903
[19] Nie Z, Yang S, Wang Y, Wang Z, Liu D, Ren Y, Chang T and Zhang R 2016 *J. Alloys Comp.* **658** 372
[20] Burzo E, Vlaic P, Kozlenko D, Kichanov S, Rutkauskas A and Savenko B 2017 *J. Alloys Compd.* **724** 1184
[21] Rietveld H 1969 *J. Appl. Cryst.* **2** 65
[22] Young R 1993 *The Rietveld Method* (Oxford, Oxford University Press) vol 5
[23] Toby B 2001 *J. Appl. Cryst.* **34** 210
[24] Larson A and Von Dreele R 2004 General Structure Analysis System (GSAS) *Los Alamos National Laboratory* LAUR 86–748
[25] Ouyang Z, Wang F, Hang Q, Liu W, Liu G, Lynn J, Liang J and Rao G 2005 *J. Alloys Comp.* **390** 21
[26] Du Z, Wang D and Zhang W 1999 *J. Alloys Compd.* **284** 206